Nucleotide excision repair : complexes and complexities : a study of global genome repair in human cells

Volker, Marcel

Appendix
Selected colour figures

Global genome repair in chromatin

Access, repair, restore

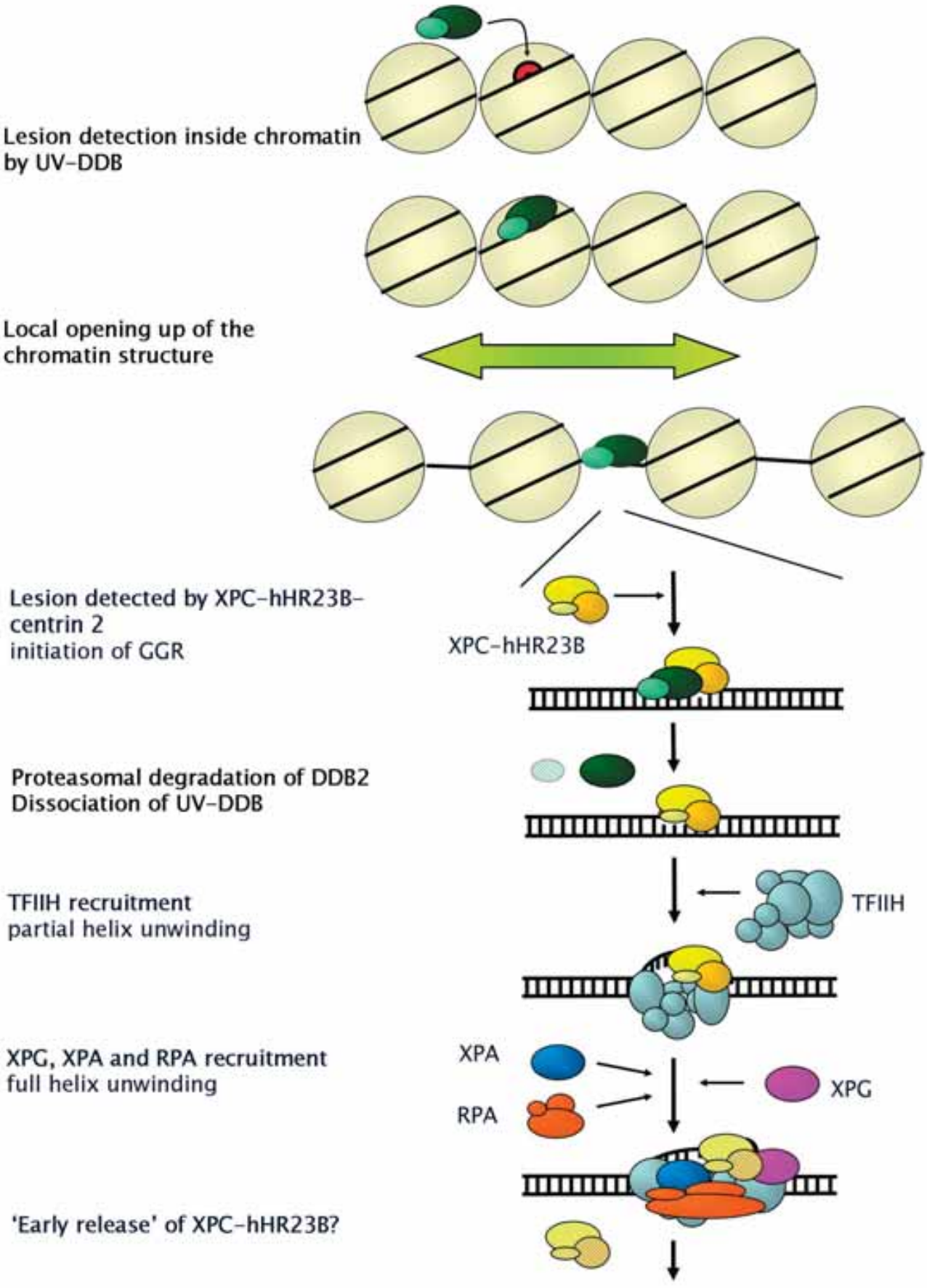

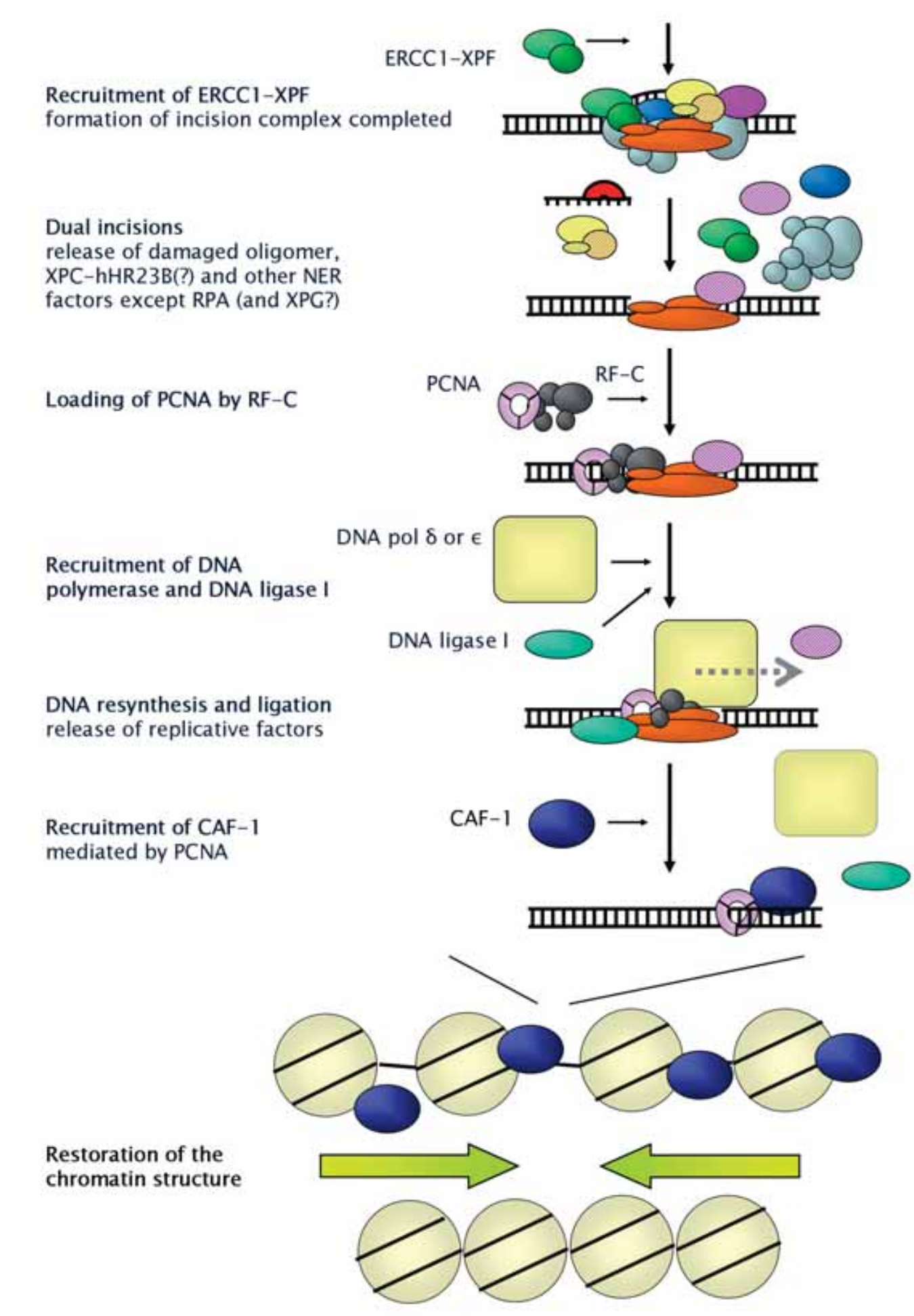
ERCC1-XPF
Recruitment of ERCC1-XPF
formation of incision complex completed
Dual incisions
release of damaged oligomer,
XPC-hHR23B(?) and other NER
factors except RPA (and XPG?)
PCNA
RF-C
Loading of PCNA by RF-C
DNA pol δ or ϵ
Recruitment of DNA
polymerase and DNA ligase I
DNA ligase I
DNA resynthesis and ligation
release of replicative factors
CAF-1
Recruitment of CAF-1
mediated by PCNA
Restoration of the
chromatin structure

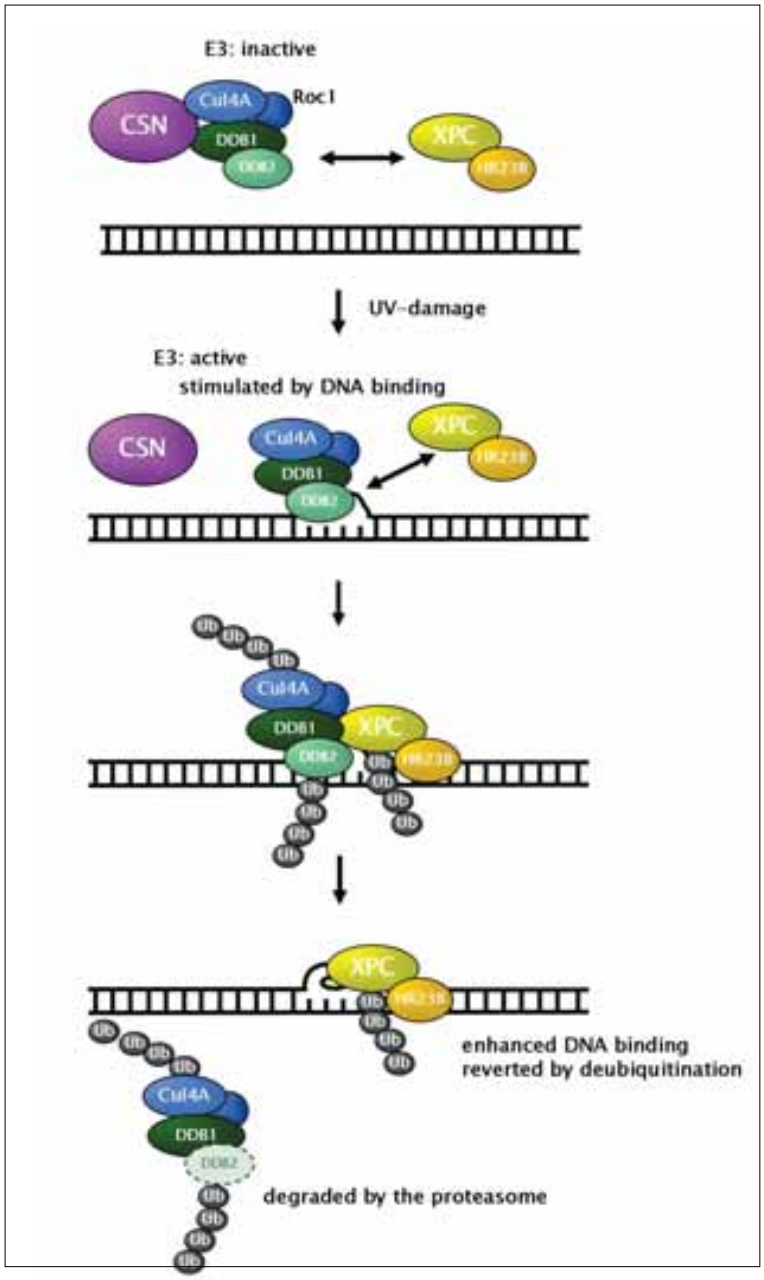

Chapter 3, Figure 2. UV-induced UV-DDB-dependent ubiquitination of XPC

In unirradiated cells, the UV-DDB-associated E3 is inactivated by its interaction with the COP9 signalosome (CSN). Thus, XPC is not ubiquitinated, despite its interaction with UV-DDB. Upon UV irradiation, UV-DDB binds to lesions, particularly 6-4PP. CSN dissociatiates from E3, activating it.

The binding of UV-DDB to the lesion further stimulates E3 activity. The activated UV-DDB-E3 then recruits XPC, and XPC and DDB2 are ubiquitinated at the lesion site. Polyubiquitinated UV-DDB loses its damaged DNA binding activity, whereas the DNA binding of XPC is enhanced by its ubiquitination. This results in the displacement of UV-DDB by XPC on the lesion. Ubiquitinated DDB2 is degraded by the proteasome. The ubiquitinated form of XPC reverts to the unmodified form through deubiquitation. Adapted from Sugasawa et al., 2005.

Previous pages: Chapter 3, Figure 1. Global genome repair inside chromatin – access, repair, restore

Schematic depiction of GGR placed within the context of chromatin. Upon lesion recognition (at least for UV lesions this is likely to involve UV-DDB, but other lesions may also be recognised by UV-DDB), chromatin remodelling enzymes are recruited to the lesion site. Local opening of the chromatin structure provides access for the core GGR machinery, and the lesion is bound by the essential damage recognition factor XPC-hHR23B (which in vivo is associated with centrin 2). XPC-hHR23B(-centrin 2) slightly opens up the DNA around the lesion and recruits TFIIH. This factor uses its two helicases, XPB and XPD, to fully open up the helix, and subsequently XPA, RPA and XPG are recruited. RPA binds to the single-strand DNA formed by the consecutive actions of XPC-hHR23B(-centrin 2) and TFIIH; XPA is the damage verification protein and XPG is one of the two structure-specific endonucleases employed by NER. Some reports suggest that at this stage, XPC-hHR23B (-centrin 2) is released from the complex (Wakasugi and Sancar, 1998; Riedl et al., 2003); however in our experiments we were unable to provide support for this notion (chapter 10). The recruitment of XPA is a prerequisite for the incorporation of the second structure-specific endonuclease, ERCC1-XPF into the complex, completing the formation of the preincision complex. The next step in the repair reaction is dual incision, followed by the release of several, but not all, repair factors. RPA remains bound to the single-strand DNA, as may XPG (which contains a PCNA-binding motif). The latter stages of repair are carried out by proteins also functioning during DNA replication: RF-C loads PCNA onto the DNA, DNA polymerases δ or ε can synthesise across the gap, and DNA ligase I is able to seal the remaining nick. Post-repair restoration of the chromatin structure involves CAF1, recruited to the site of repair by PCNA which has remained bound to the DNA. See text for details.

Chapter 6, Figure 1. Altered Nuclear Distribution of TFIIH in Confluent Human Fibroblasts after Global UV Irradiation

(A) Growing or confluent normal human fibroblasts (VH25) were fixed and immunolabeled employing an antibody against XPB or immunolabeled at 30 min after UV irradiation (10 J/m^2). (B) Confluent normal human (VH25), CS-B (CS1AN), XP-A (XP25RO), and XP-C (XP21RO) fibroblasts were either fixed and immunolabeled using an antibody against XPB or exposed to UV (10 J/m^2) and immunolabeled 30 min or 2 hr later.

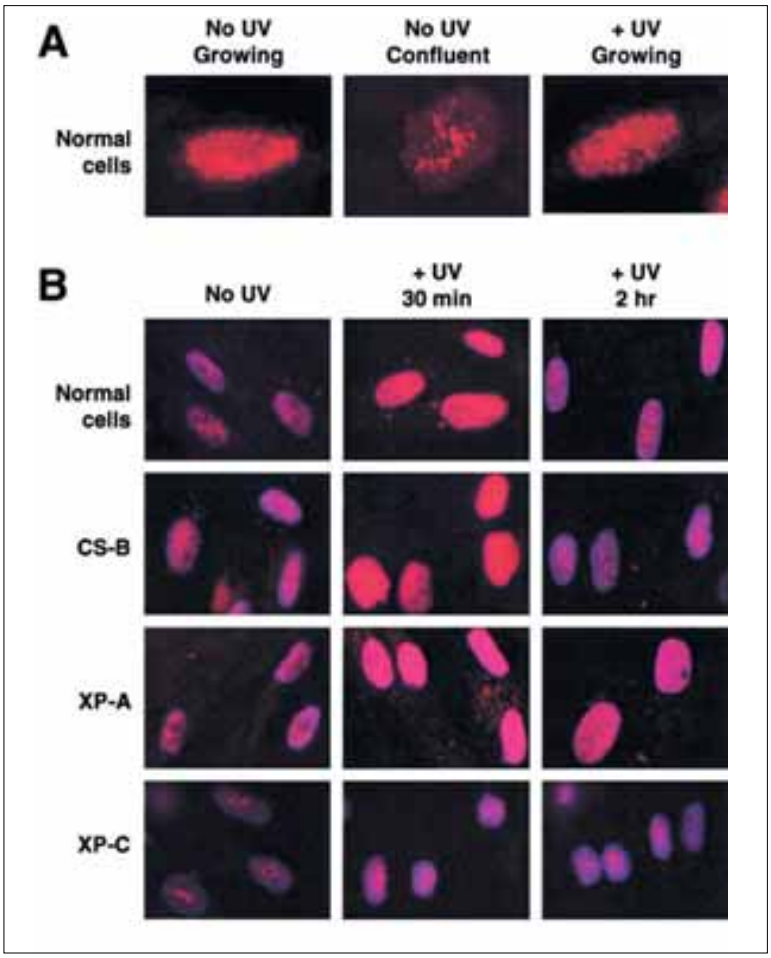

Chapter 6, Figure 3. UV Exposure through Isopore Polycarbonate Filters Causes Locally Damaged Areas in the Nuclei

Normal human fibroblasts (VH25) were UV-irradiated with 20 or 30 J/m^2 through a 3 or 8 µm pore filter and immediately fixed. Immunofluorescent labeling was performed using (A) an antibody against CPD (α-CPD) or (B) an antibody against 6-4PP (α-64PP). In addition (C), VH25 cells were locally exposed to UV radiation, incubated for 20 min in culture medium, and permeabilized, after which run-on DNA synthesis in the presence of biotin-dUTP was carried out. Cells were subsequently immunolabeled for both DNA repair synthesis (biotin-16-dUTP) and the presence of DNA damage, i.e., 6-4PP (α-64PP).

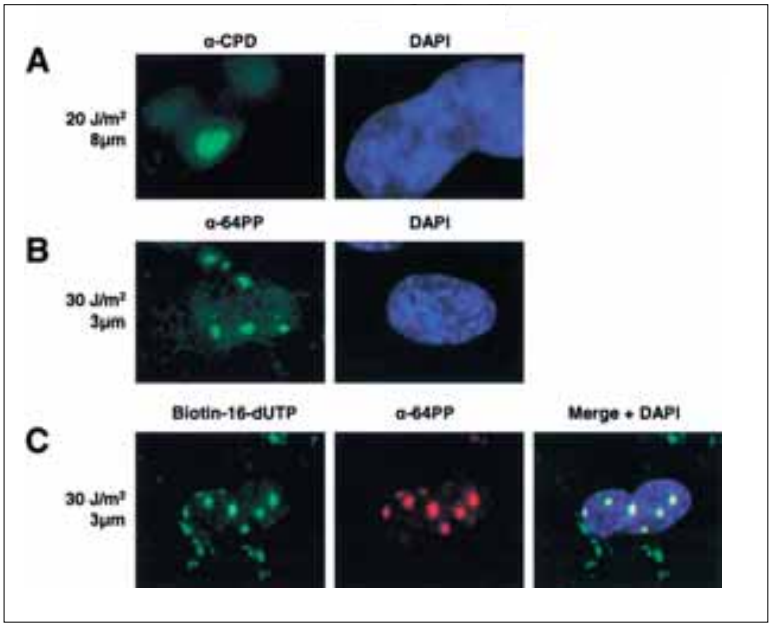

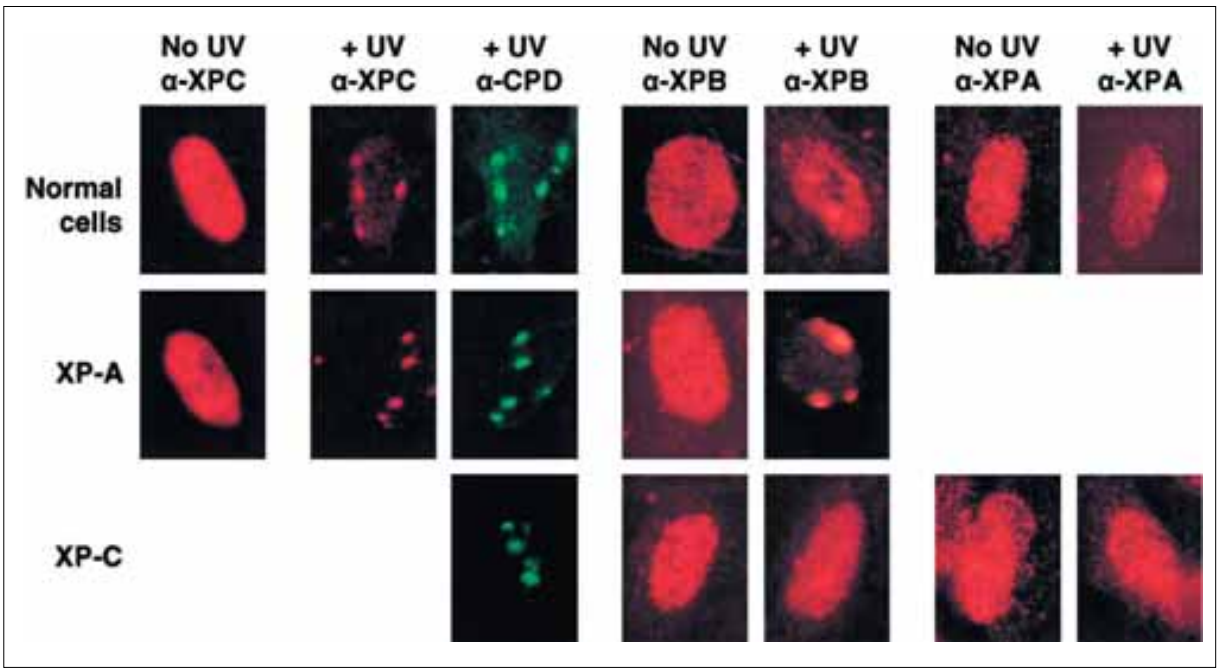

Chapter 6, Figure 4. Recruitment of NER Proteins to Sites of UV Damage

Normal human (VH25), XP-A (XP25RO), and XP-C (XP21RO) fibroblasts were UV exposed to 30 J/m^2 through 3 µm filters or mock irradiated and at 15 min after exposure immunolabeled with an antibody (red) against XPC and an antibody (green) against CPD or labeled with antibodies against XPB or XPA.

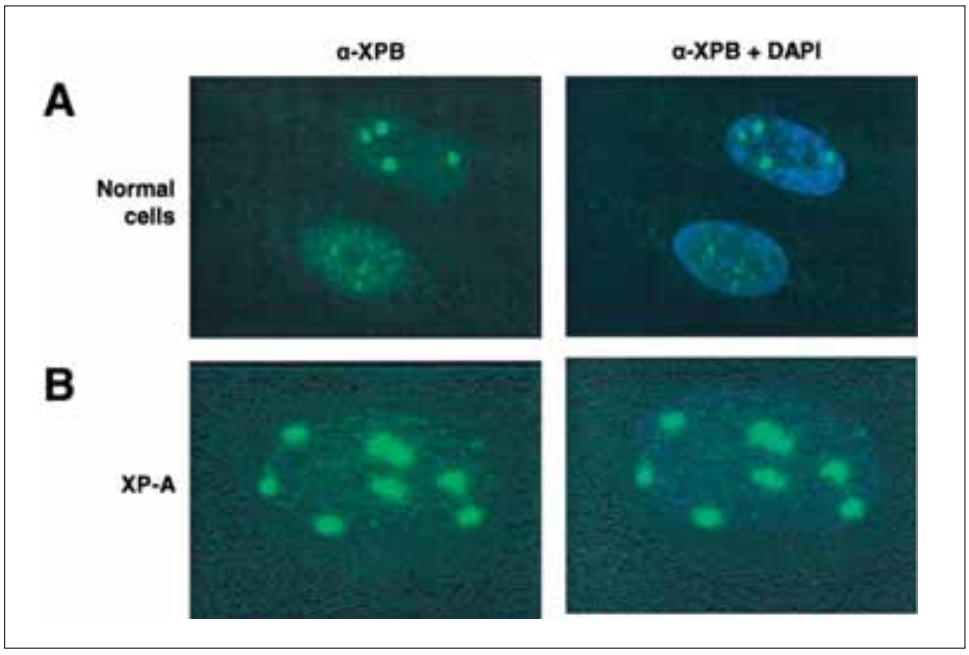

Chapter 6, Figure 5. Reduction of XPB in Unexposed Parts of the Nucleus after Local UV Irradiation

Normal human fibroblasts (VH25) (A) or XP-A cells (XP25RO) (B) were UV irradiated with 30 J/m^2 through 3 µm pore filters and immunolabeled for XPB 15 min or 4 hr after UV exposure, respectively.

Chapter 6, Figure 6. Recruitment of the NER Endonucleases to the Sites of UV Damage

Confluent fibroblasts were UV irradiated (30 J/m^2) through 3 µm filters or mock irradiated, fixed 15 min after UV exposure and immunolabeled for ERCC1, XPG, or XPA. (A) Unexposed normal human fibroblasts (VH25) were immunolabeled for ERCC1 and XPG. (B) Normal human (VH25), XP-A (XP25RO), and XP-C (XP21RO) fibroblasts were immunolabeled for ERCC1 and XPG. (C) XP-F (XP24KY) and XP-G (XPCS1RO) fibroblasts were immunolabeled for XPG and ERCC1, respectively, or XPA.

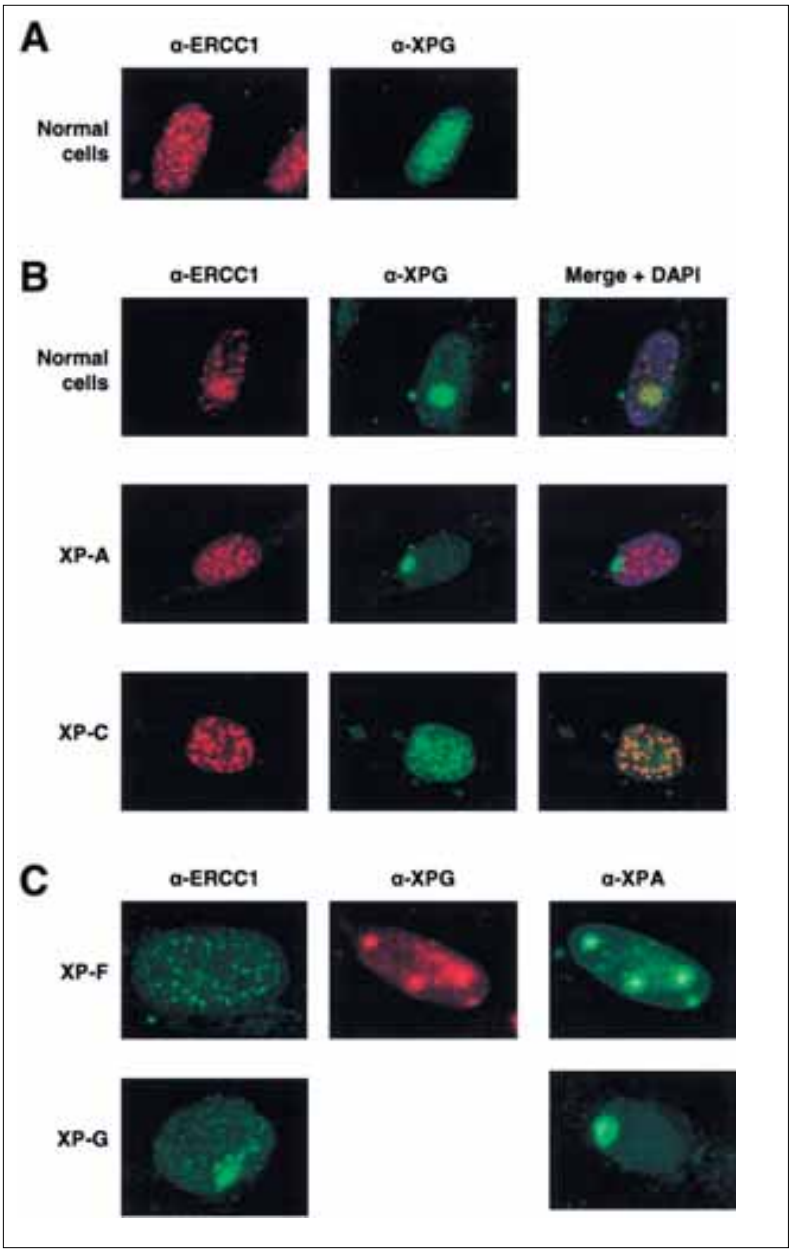

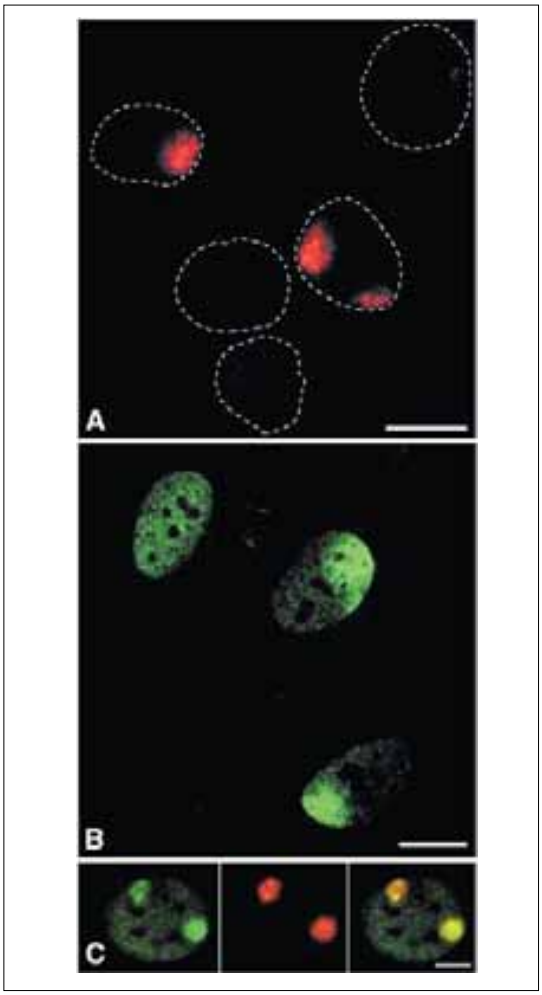

Chapter 7, Figure 1

(A) Detection of locally induced UV damage in cell nuclei. A UV-blocking polycarbonate filter containing pores of 5 µm in diameter was used to cover a monolayer of cells. The filter-covered cells were UV-irradiated with 30 J/m^2 and CPDs were subsequently detected by immunofluorescent labelling. Dotted lines denote the contours of individual cell nuclei. Two nuclei show labelling of CPDs in discrete nuclear areas. (B) Effect of local nuclear UV damage on the distribution of TFIIH. Human primary fibroblasts were locally UV-irradiated with 100 J/m^2 UV light, using a filter with 10 µm pores. Following irradiation, cells were grown for 1 h and immunolabelled against the p62 subunit of TFIIH. The top-left nucleus displays the characteristic labelling pattern of TFIIH in unirradiated cells, whereas the two remaining nuclei exhibit a TFIIH accumulation in UV-damaged nuclear areas, and a reduction in TFIIH signal outside these areas. A single confocal optical section is shown. (C) Colocalization of TFIIH (green) and CPDs (red). Human primary fibroblasts were locally irradiated with 30 J/m2 UV light, using a filter with 8 µm pores. Following irradiation, cells were grown for 30 min and dual labelled against both CPDs and the p62 subunit of TFIIH. Bars represent 10 µm.

Chapter 7, Figure 2. Effect of local nuclear UV damage on transcription

Normal human primary fibroblasts (WT; NER-proficient) and immortalized primary fibroblasts from patients suffering from xeroderma pigmentosum group A (XP-A; no NER), group C (XP-C; no GGR) or Cockayne syndrome group B (CS-B; no TCR) were studied.

Exponentially growing cells were locally UV-irradiated with 50 J/m^2 using filters containing 10 µm pores. After irradiation, cells were cultured for either 1 or 12 h. Subsequently, cells were allowed to incorporate BrUTP into nascent RNA during run-on transcription labelling. Nascent RNA (green) and CPDs (red) were dual labelled by immunostaining. Single confocal optical sections are shown. Bars represent 5 µm.

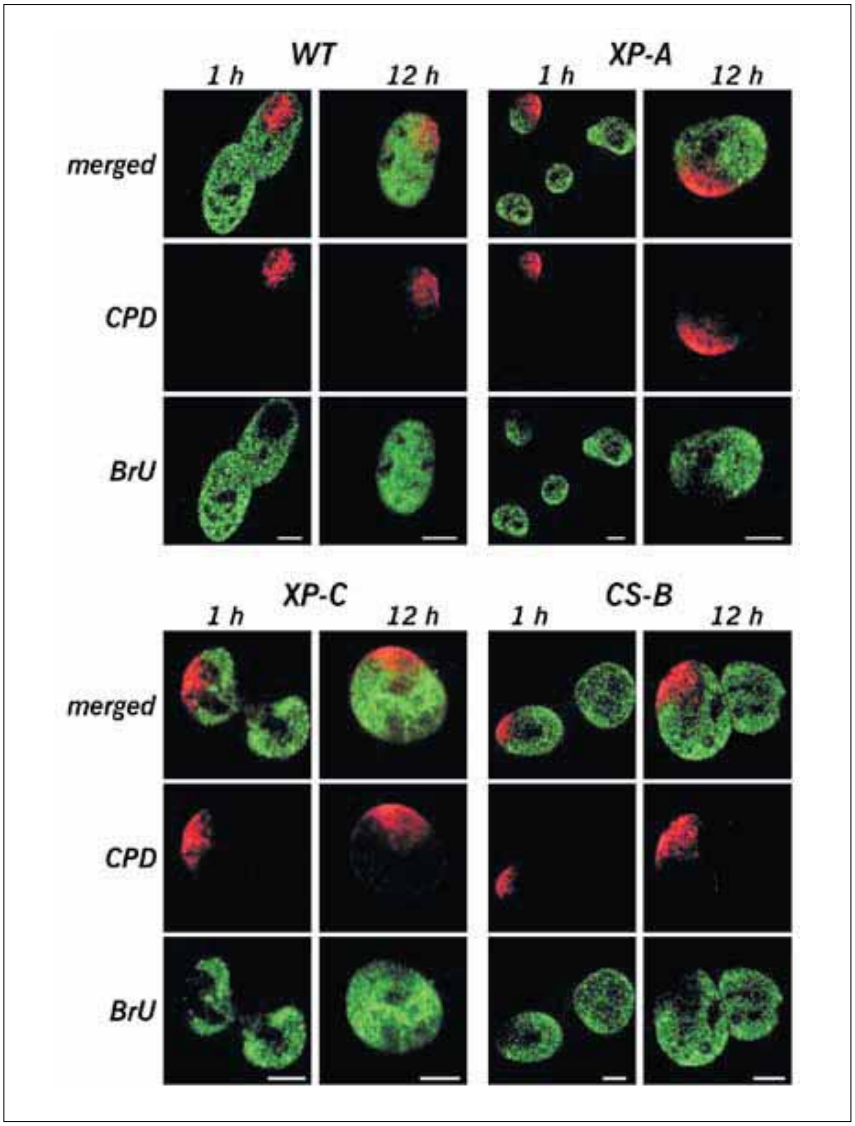

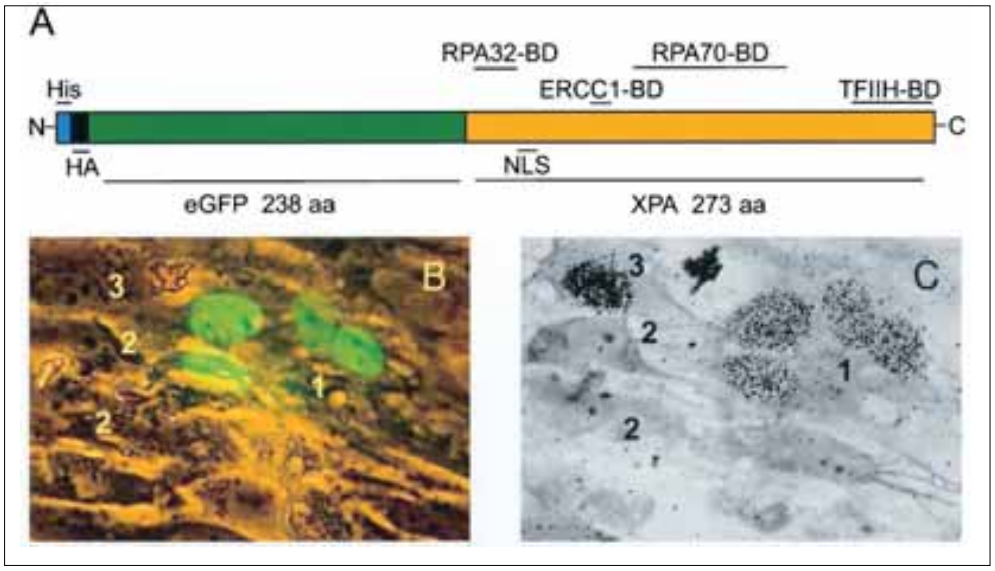

Chapter 8, Figure 1. Functionality of GFP-XPA

(A) Schematic representation of the His9-HA-eGFP–XPA fusion gene with the different binding domains indicated. NLS, nuclear localization signal; BD, binding domain; aa, amino acids. (B) Fluorescence image of XP-A cells injected with GFP-tagged XPA cDNA. Only the multinucleated cell microinjected with GFP-XPA cDNA showed a homogeneous nuclear expression (number 1); surrounding cells were not injected (number 2). (C) Measurement of the repair capacity of cells with fluorescent nuclei by means of UV-induced UDS (see Materials and Methods). The amount of silver grains above the nuclei of the injected cells (number 1) was comparable to what was seen with wild-type cells (not shown), whereas the surrounding XP-A fibroblasts (number 2) show the low level of DNA synthesis typical for UV-exposed XP-A cells. The cell indicated with the number 3 is in S phase.

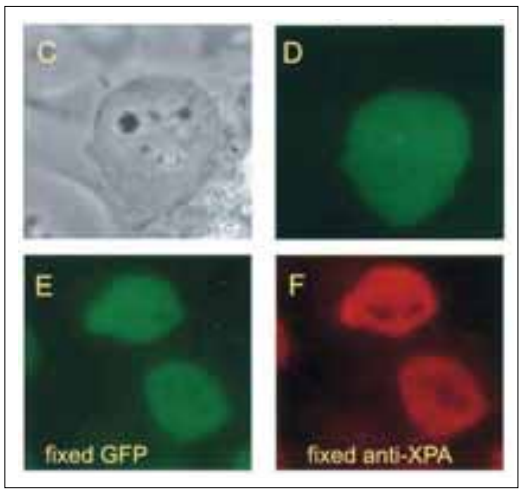

Chapter 8, Figure 2. Expression and characterization of XP2OS cells stably expressing GFP-tagged XPA

(C) Phase-contrast image of a living GFP-XPA-transfected XP2OS, clone 40 cell. (D) Epifluorescence GFP image of the same cell as in panel C, showing a homogeneous nuclear distribution. (E) Fluorescence image after fixation of clone 40, showing a similar distribution as in panel D. (F) Immunofluorescence of the same cell as in panel E incubated with anti-XPA serum, showing a similar XPA distribution as with GFP fluorescence, except for the nucleoli.

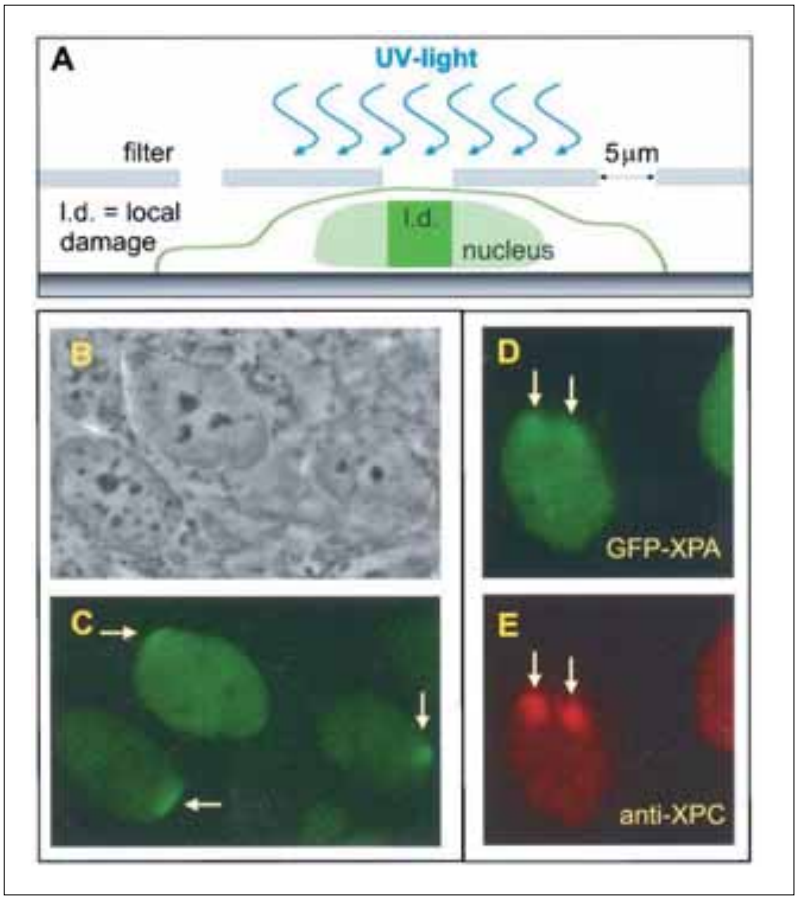

Chapter 8, Figure 5. Accumulation of GFP-XPA within restricted nuclear areas after local UV irradiation

(A) Schematic presentation of local UV damage infliction on living cultured cells. (B and C) Micrographs, phase-contrast image [B] and fluorescence image [C] of living cells expressing GFP-XPA (clone 40) and UV-irradiated through a filter with small (5 μm-diameter) pores. The arrows in panel C point to the local accumulations of GFP-XPA. (D and E) GFP-XPA accumulations (arrows) shown in panel D clearly colocalize with endogenous XPC (E) concentrations, as determined with anti-XPC antibodies, in fixed cells.

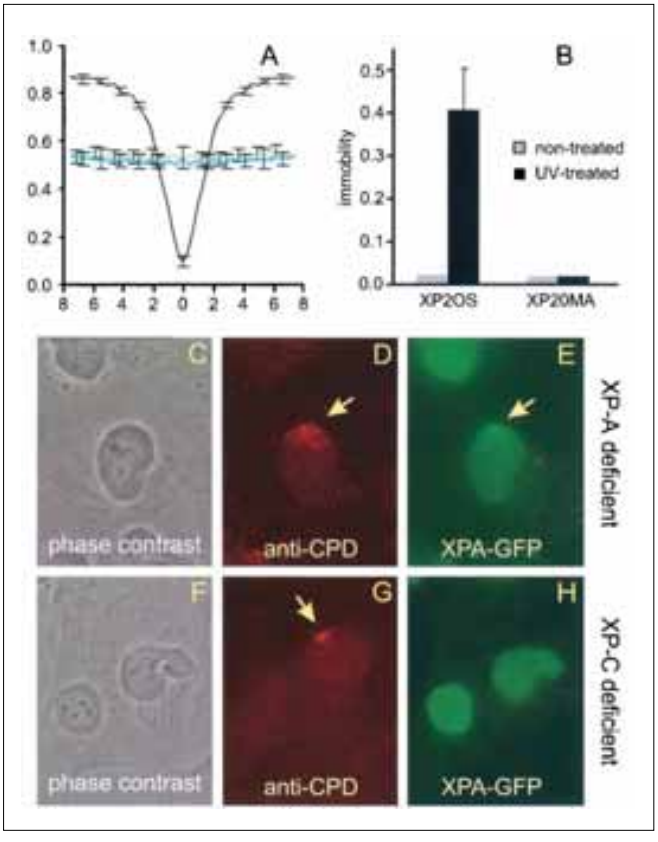

Chapter 8, Figure 7. Effect of XPC on damage-induced XPA immobility as analyzed by FRAP-FIM and local damage induction

(A) FRAP-FIM profile of GFP-XPA expression in XP20MA (XP-C) cells. Shown are results for nonirradiated cells (light green line), cells irradiated at 16 J/m^2 (blue line), and fixed cells (black line). UV-exposed XP20MA cells do not show any GFP-XPA immobilization. (B) Quantification of immobilization of GFP-XPA in XP20MA and XP2OS cells with and without UV irradiation. (C) Phase-contrast image of GFP-XPA-expressing XP2OS cells. (D) Anti-CPD immunostaining in a GFP-XPA-expressing XP2OS cell. The arrow indicates the site of the damage. (E) GFP image of the same cell as in panel D, showing enrichment of GFP-XPA at the damaged site. (F) Phase-contrast image of GFP-XPA-expressing XP20MA cells. (G) Anti-CPD immunostaining of a GFP-XPA-expressing XP20MA cell, indicated by the arrow. (H) GFP image showing no enrichment of GFP-XPA molecules.

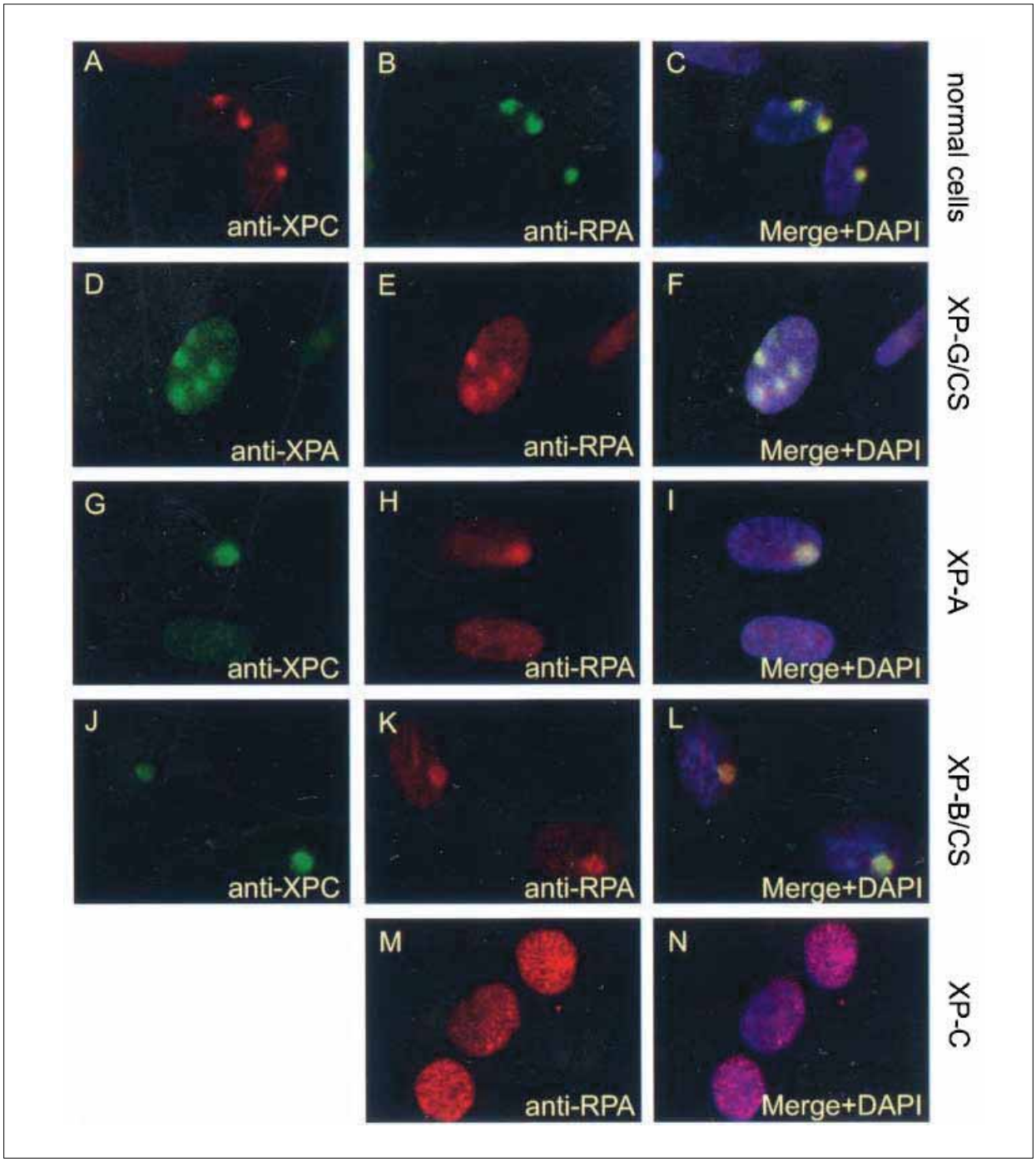

Chapter 8, Figure 8. Relocalization of RPA to the NER complex 30 min after local irradiation with 25 J/m² UV

(A to C) Anti-XPC (A) and anti-RPA (B) immunostaining of VH25 cells and the merged image after immunostainings plus DAPI nuclear DNA staining (C). (D to F) Anti-XPA (D) and anti-RPA (E) immunostaining of XPCS1RO cells and the merged image after immunostainings plus DAPI nuclear DNA staining (F). (G to I) Anti-XPC, G and anti-RPA (H) immunostaining of XP25RO cells and the merged image after immunostainings plus DAPI nuclear DNA staining. (J to L) Anti-XPC (J) and anti-RPA (K) staining of XP131MA cells and the merged image after immunostainings plus DAPI nuclear DNA staining (L). (M and N) Anti-RPA immunostaining of XP21RO cells (M) and the merged image after immunostaining plus DAPI nuclear DNA staining (N). The yellow color in the merged images in panels C, F, I, and L indicates colocalization of NER proteins at sites of locally induced DNA damages.

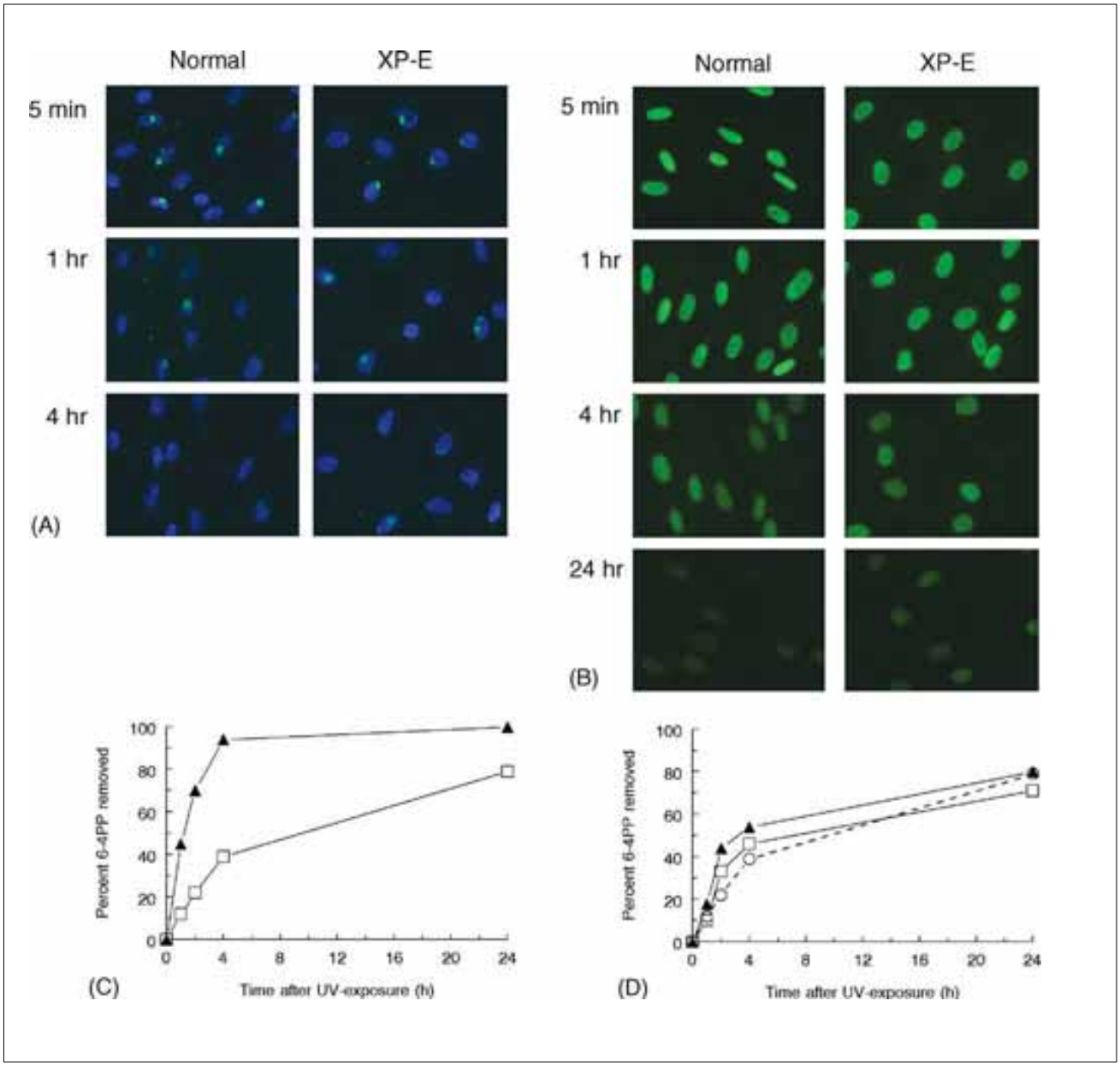

Chapter 9, Figure 3. Accelerated 6-4PP repair in normal human fibroblasts (VH10hTert) compared to XP-E fibroblasts (GM01389hTert) after local UV irradiation, but not after global UV irradiation as measured by immunofluorescence

(A) Fluorescent immunostaining of 6-4PP (green) at various times after local UV irradiation (30 J/m^2) through an 8 µm pore size filter. Images were taken with equal exposure times and merged with DAPI nuclear DNA staining (blue). (B) Fluorescent immunostaining of 6-4PP (green) at various times after global UV irradiation (30 J/m^2). Images were taken with equal exposure times. (C and D) Graphs presenting the percentage of 6-4PP removed determined from multiple (>20) fluorescent images for each timepoint. (C) Removal of 6-4PP in (▲) normal human and (□) XP-E cells following exposure to 30 J/m^2 of local UV irradiation through an 8 µm pore size filter. (D) Removal of 6-4PP in (▲) normal human and (□) XP-E cells following exposure to 30 J/m^2 of global UV. The dotted line is taken from C showing removal of 6-4PP in XP-E cells which were locally UV-irradiated with 30 J/m^2 and is depicted as a reference. Signal intensities were determined by measuring the total fluorescence intensity of a spot or a nucleus, and dividing by the surface area of the measured spot or nucleus, respectively.

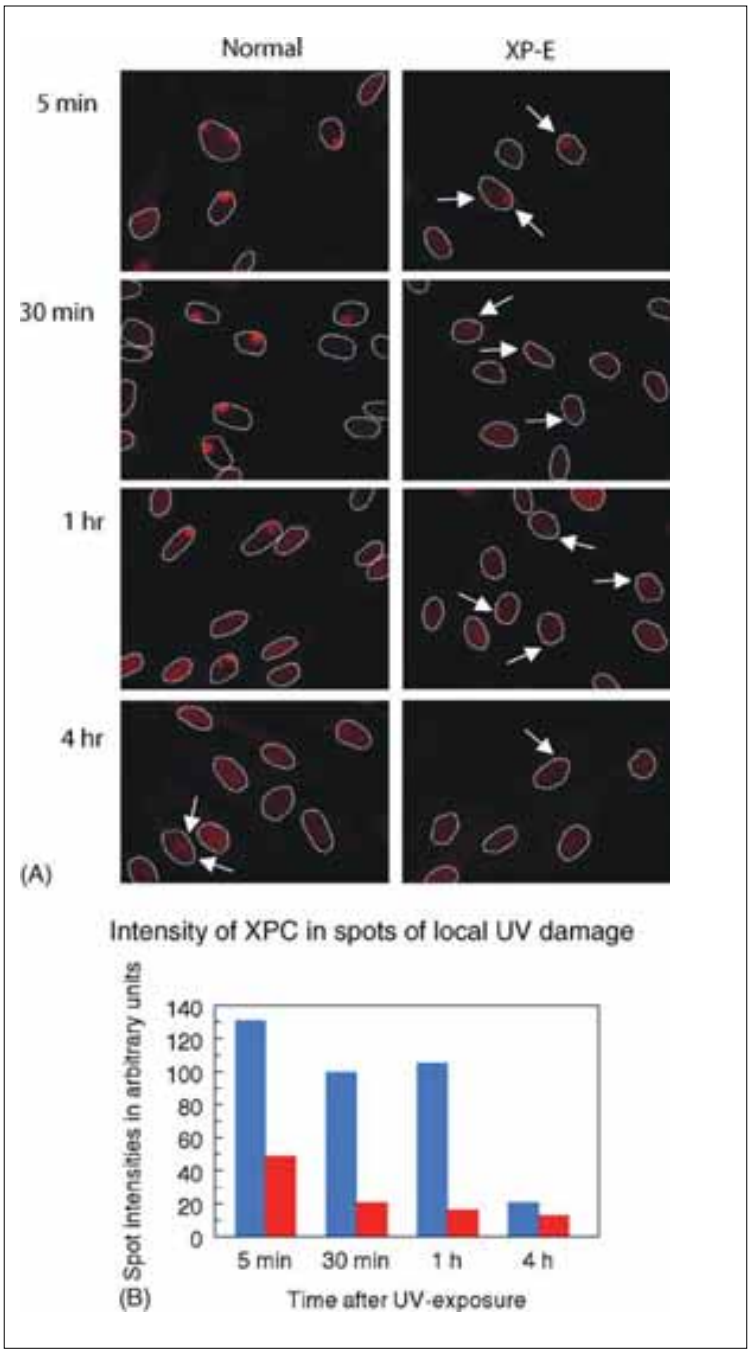

Chapter 9, Figure 5. XPC accumulates differentially in normal human fibroblasts (VH10hTert) and XP-E fibroblasts (GM01389hTert) after local UV irradiation

Cells were UV-irradiated with 20 J/m^2 through an 8 µm pore size filter. (A) Fluorescent immunostaining of XPC (red) at various times after irradiation. Arrows indicate protein accumulations in UV-damaged spots that are poorly visible. Dotted lines outline the nuclei as determined from DAPI nuclear counterstaining (images not shown). All fluorescent images were taken with equal exposure times. (B) Bar graph showing average intensities of XPC spots at various time points after irradiation (blue bars: normal cells; red bars: XP-E cells). Spot intensities were determined by measuring the total fluorescence intensity of a spot, divided by its surface area, and corrected for background levels of fluorescence in the nucleus. For each time point, at least 20 cells were measured. The fluorescent signal measured 30 min after UV in normal human cells was set to 100%.

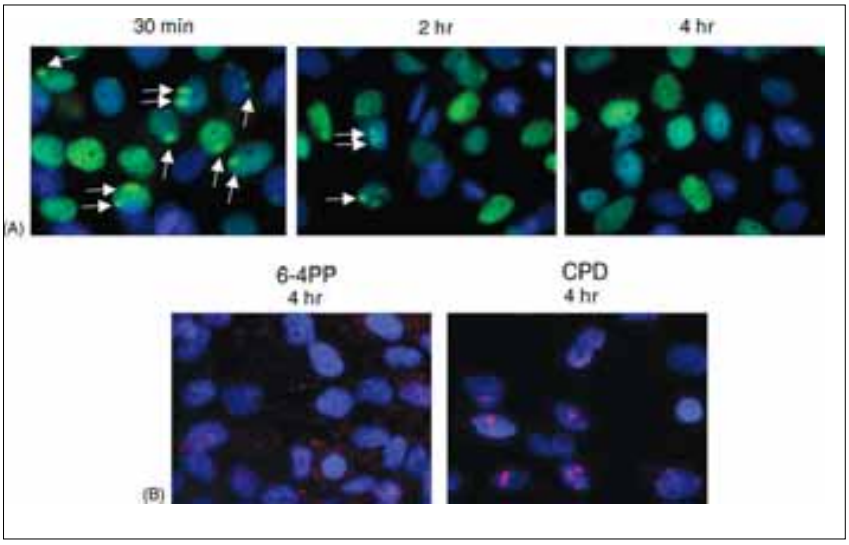

Chapter 9, Figure 7. Formation of p48 spots after induction of local UV damage coincides with 6-4PP repair

Normal human cells (MRC5) stably expressing p48-YFP were exposed to 30 J/m^2 of UV through a 5 µm pore size filter. (A) Fluorescent images of p48-YFP (green) merged with DAPI nuclear DNA staining (blue) taken at various times following irradiation. Arrows indicate sites of local UV damages. Pictures were taken with equal exposure times. (B) Fluorescent immunostaining using anti-CPD antibody (red) or anti-6-4PP antibody (red) 4 h after exposure, merged with DAPI nuclear DNA staining (blue).

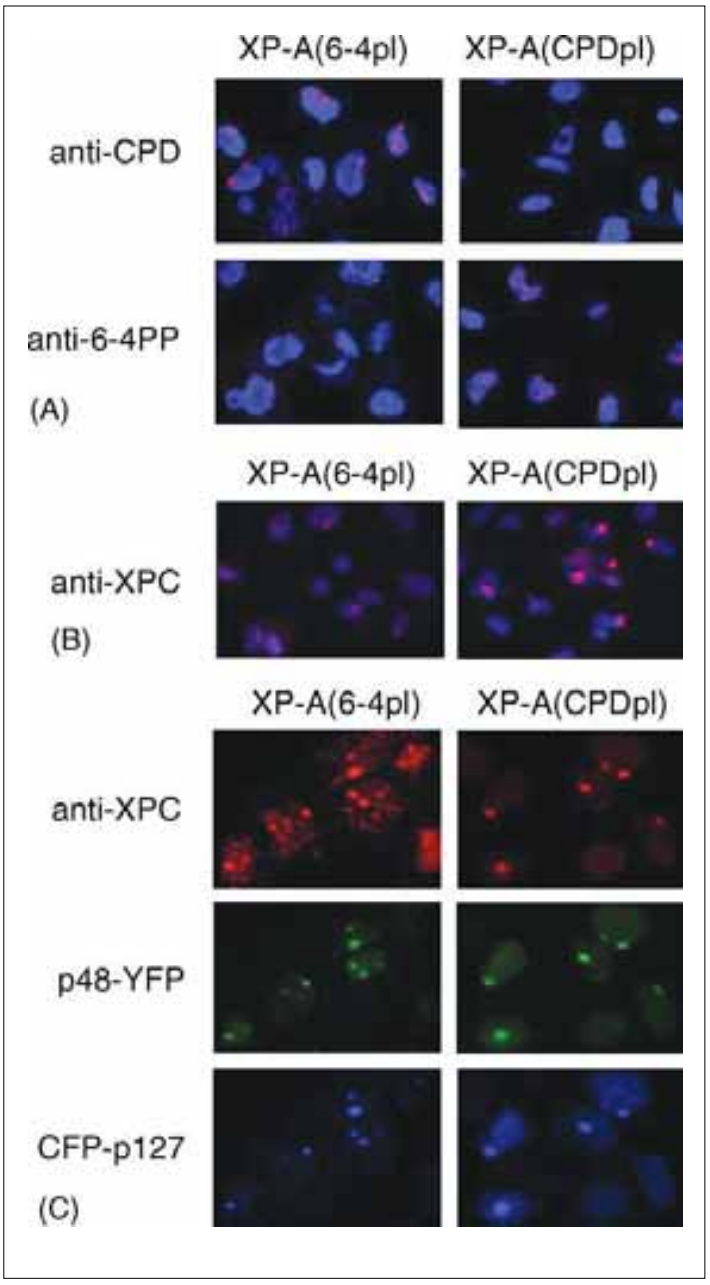

Chapter 9, Figure 8. Accumulation of XPC, p48 and p127 in local UV-damaged spots after removal of one of the two types of UV-photolesion by photoreactivation

XP-A cells stably expressing 6-4PP photolyase [XP-A(6-4)phl)] or CPD photolyase [XP-A(CPDphl)], respectively, were irradiated with 30 J/m^2 of UV through a 5 µm pore size filter, and exposed to photoreactivating light for 1 h. (A) Fluorescent immunostaining of CPD (red) and 6-4PP (red), merged with DAPI nuclear DNA staining. (B) Fluorescent immunostaining of XPC after photoreactivation of 6-4PP (left) or CPD (right) in XP-A photolyase expressing cells. Pictures taken with equal exposure times and merged with DAPI nuclear counterstaining (blue). (C) XP-A(6-4)phl or XP-A(CPDphl) cells transfected with p48-YFP and CFP-p127 expression constructs 24 h prior to local UV-exposure and 1 h photoreactivation. Fluorescent images of XPC (using anti-XPC antibody, red), p48-YFP (green) and CFP-p127 (blue), taken with exposure times optimised for image clarity.

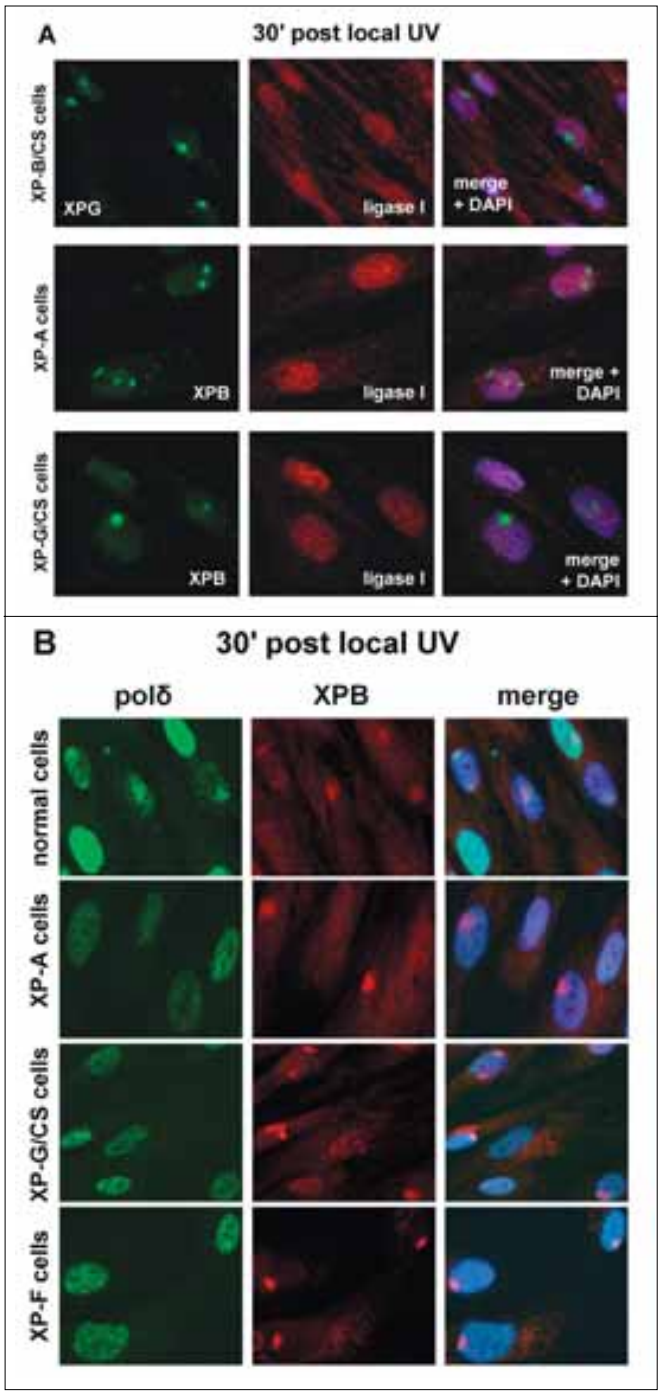

Chapter 10, Figure 2. Differential redistribution of pre- and postincision NER proteins in normal human and XP cells

NER proteins were immunofluorescently labelled in normal human and various repair-deficient XP cells 30 min following local UV treatment with 25 J/m^2.

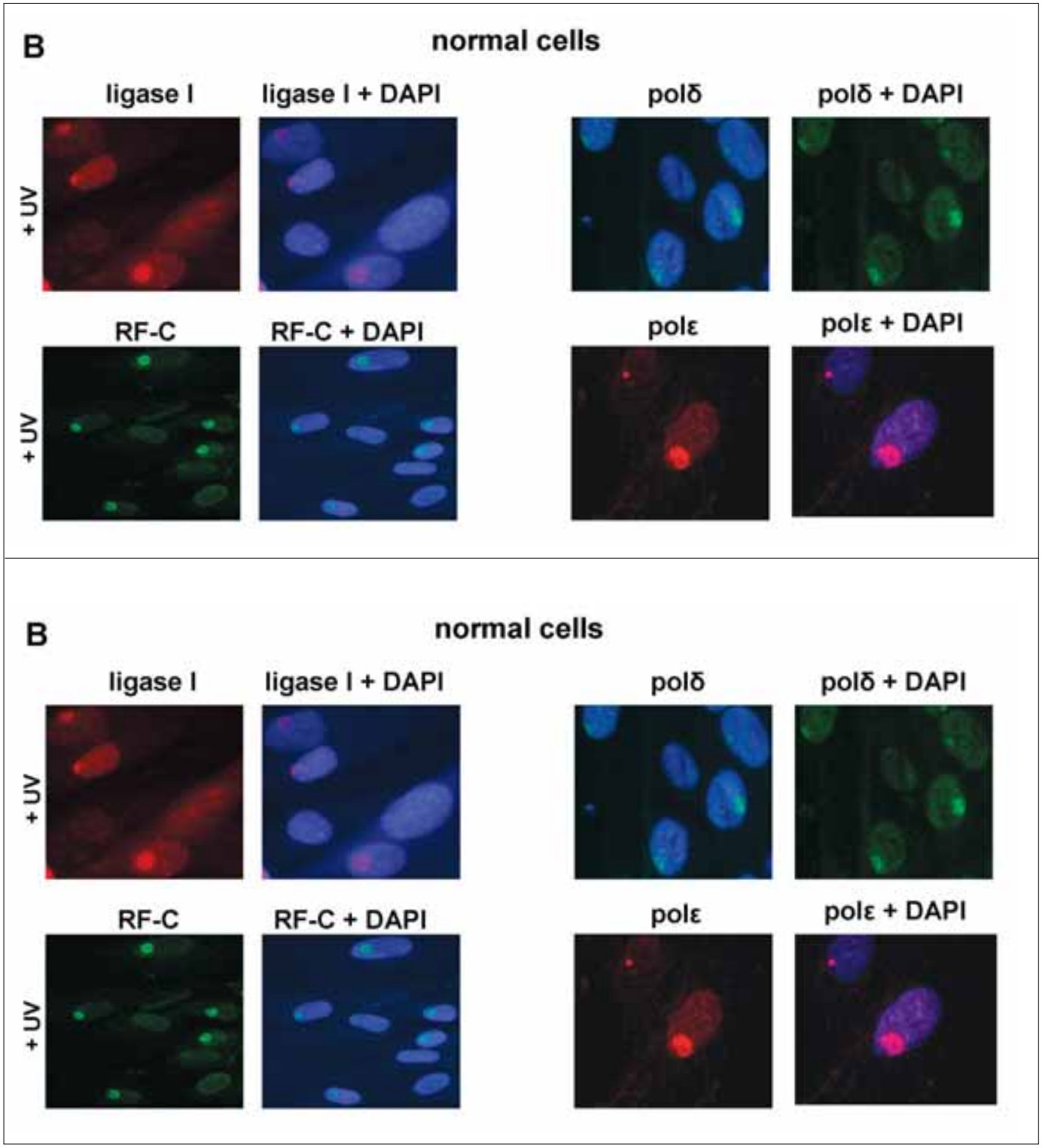

Chapter 10, Figure 1. Involvement of RF-C, polδ, polε and ligase I in NER

RF-C, polδ, polε and ligase I were immunofluorescently labelled in normal human cells. A, RF-C, polδ, polε and ligase I show a homogeneous distribution pattern prior to UV irradiation. B, 30 min following local UV irradiation with 25 J/m^2 RF-C, polδ, polε and ligase I accumulate at sites of local UV damage.

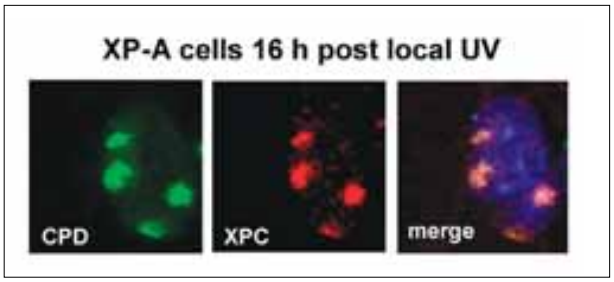

Chapter 10, Figure 3. Sustained accumulation of XPC in NER-deficient cells
XPC and CPD were immunofluorescently labelled in XP-A cells 16 hours after 25 J/m^2 local UV irradiation.

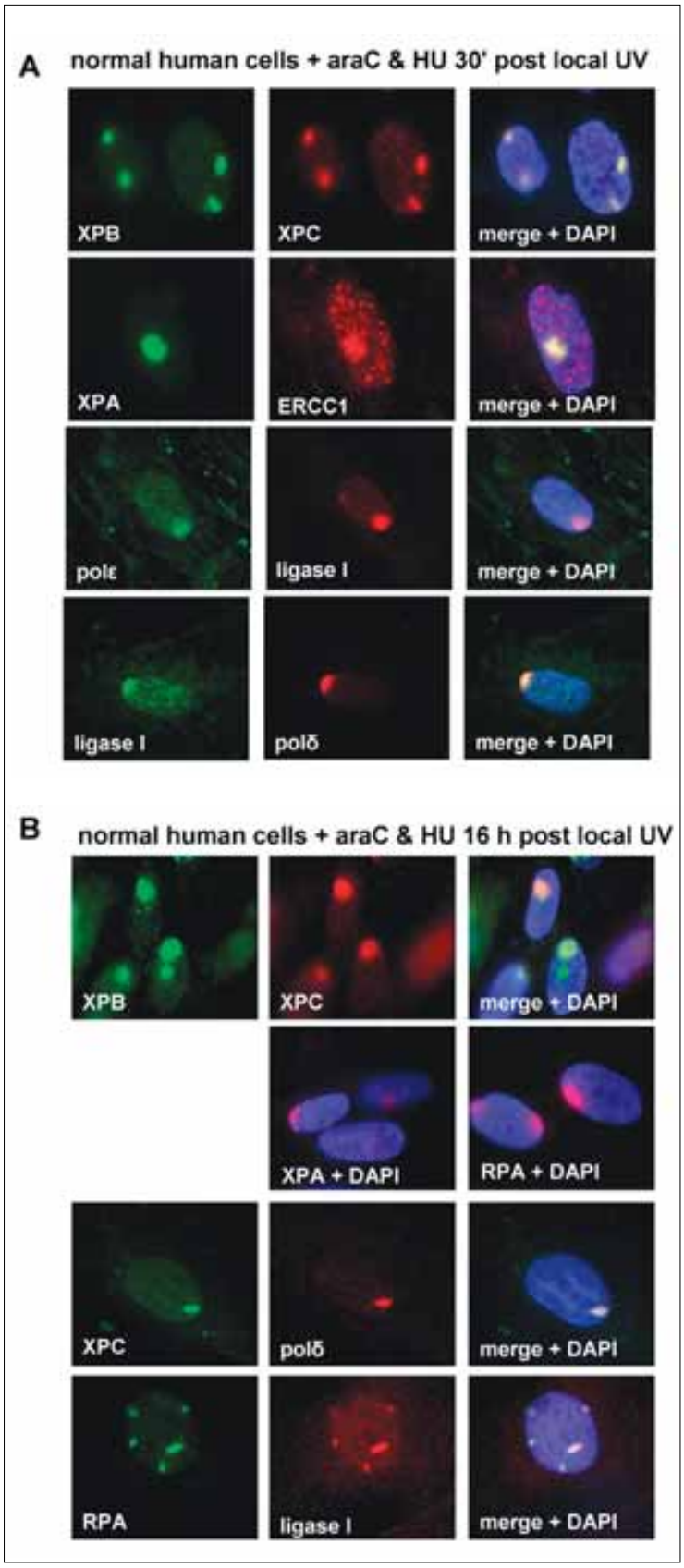

Chapter 10, Figure 4. Rapid and prolonged accumulation of NER proteins in normal human cells in the presence of araC and HU
NER proteins were immunofluorescently labelled following local UV irradiation with 25 J/m^2 in the presence of araC and HU. A, 30 min after UV. B, 16 hours after UV.

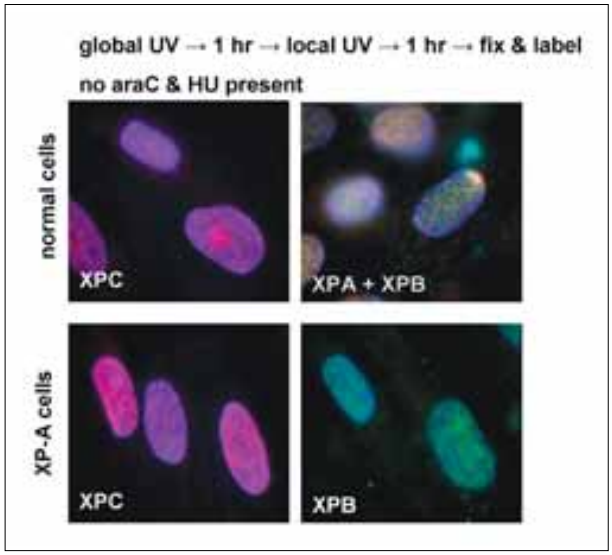

Chapter 10, Figure 5. Stability of preincision NER proteins in the NER complex in the absence of araC and HU
Normal human or XP cells were globally irradiated with 25 J/m^2, incubated for 1 hour, locally irradiated with 25 J/m^2 and incubated for another 1 hour before NER proteins were immunofluorescently labelled.

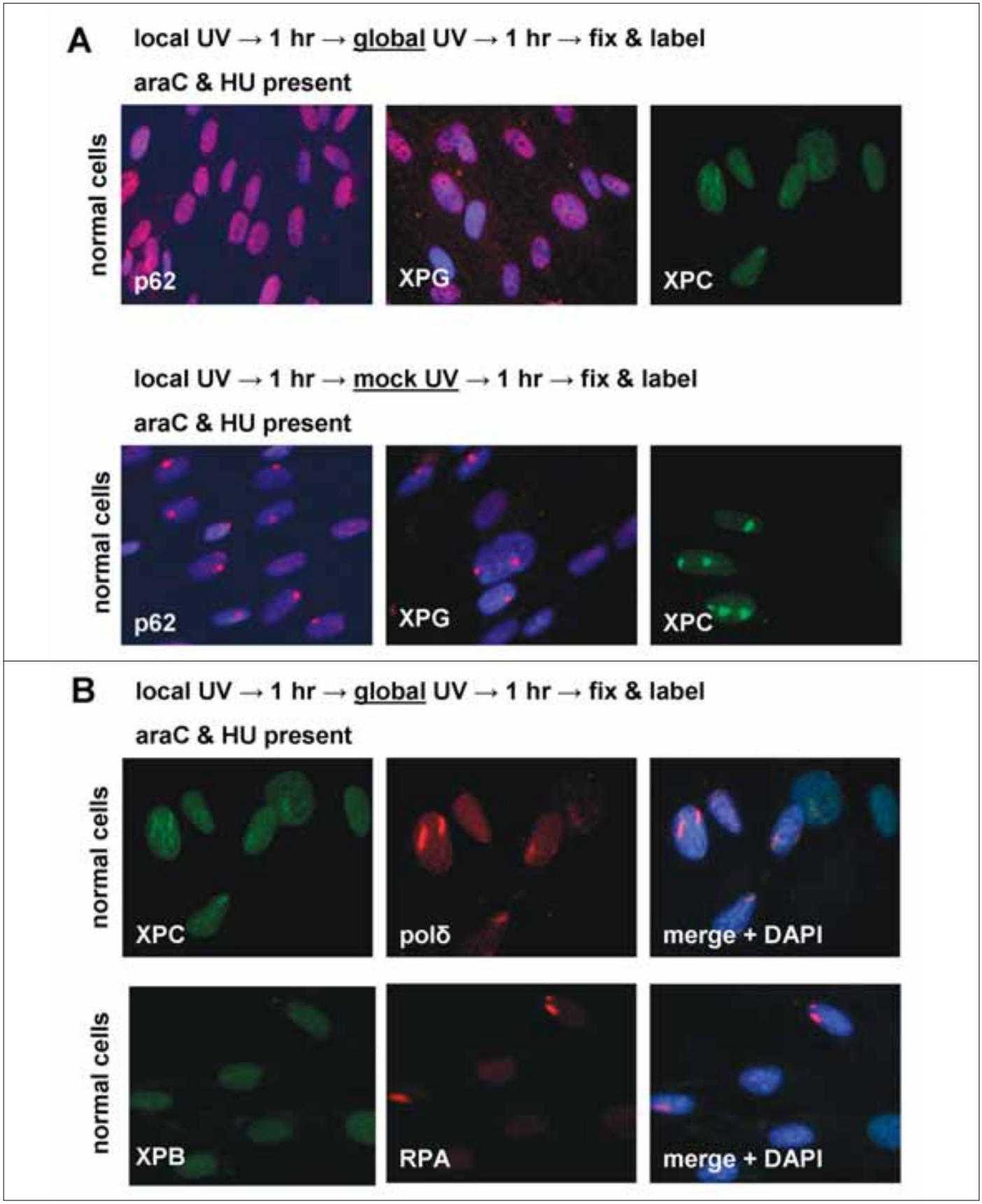

Chapter 10, Figure 6. Stability of preincision and postincision NER proteins at the site of DNA lesions in the presence of araC and HU

Normal human cells were locally irradiated with 25 J/m^2, incubated for 1 hour, globally irradiated with 25 J/m^2 and incubated for another 1 hour before NER proteins were immunofluorescently labelled. A, preincision NER proteins are tethered away from sites of primary UV damage by competition with the secondary UV lesions. B, NER proteins involved in the postincision stages remain stably associated with the primary UV lesions.